

THE REMARKABLE MID-INFRARED JET OF MASSIVE YOUNG STELLAR OBJECT G35.20-0.74

JAMES M. DE BUIZER

Gemini Observatory, Casilla 603, La Serena, Chile; jdebuizer@gemini.edu

Printed July 17, 2018

ABSTRACT

The young massive stellar object G35.20-0.74 was observed in the mid-infrared using T-ReCS on Gemini South. Previous observations have shown that the near infrared emission has a fan-like morphology that is consistent with emission from the northern lobe of a bipolar radio jet known to be associated with this source. Mid-infrared observations presented in this paper show a monopolar jet-like morphology as well, and it is argued that the mid-infrared emission observed is dominated by thermal continuum emission from dust. The mid-infrared emission nearest the central stellar source is believed to be directly heated dust on the walls of the outflow cavity. The hydroxyl, water, and methanol masers associated with G35.20-0.74 are spatially located along these mid-infrared cavity walls. Narrow jet or outflow cavities such as this may also be the locations of the linear distribution of methanol masers that are found associated with massive young stellar objects. The fact that G35.20-0.74 has mid-infrared emission that is dominated by the outflow, rather than disk emission, is a caution to those that consider mid-infrared emission from young stellar objects as only coming from circumstellar disks.

Subject headings: circumstellar matter — infrared: ISM — stars:formation — ISM: individual (G35.20-0.74) — ISM: jets and outflows — masers

1. INTRODUCTION

While molecular outflows are an apparently ubiquitous phenomena in regions of high-mass star formation (Shepherd and Churchwell 1996; Zhang et al. 2001; Beuther et al. 2002), clear examples of individual young massive stars with well-defined bipolar jets are relatively few. One such example is G35.20-0.74, a massive star formation region containing an early B-type star surrounded by an ultra-compact HII region (UCHII region) with a bipolar jet-like radio structure. Water, OH, and methanol masers (Forster & Caswell 1989, Hutawarafor & Cohen 1999) are all associated with this massive young stellar object, though the nature of their relationship with respect to G35.20-0.74 is still unclear.

This jet and outflow have recently been observed in the near-infrared (NIR) by Fuller, Zijlstra, & Williams (2001) and in the mid-infrared (MIR) at low spatial resolution ($\sim 1''$) by De Buizer et al. (2005). The nature and structure of the thermal infrared emission seen from this outflow in these two studies has prompted this high spatial resolution ($\sim 0.35''$ at $11.7\mu\text{m}$) MIR follow-up study. In this Letter, I will explore the characteristics of the MIR emission in G35.20-0.74 and relationships between the detailed morphologies of the infrared emission, masers, and radio continuum emission.

2. OBSERVATIONS

Observations of G35.20-0.74 were carried out at Gemini South on the night of 2005 July 12 through patchy clouds. Imaging was performed with the Thermal-Region Camera and Spectrograph (T-ReCS) using the *Si-5* ($\lambda_c=11.7\mu\text{m}$, $\Delta\lambda=1.1\mu\text{m}$) filter and *Qa* filter ($\lambda_c=18.3\mu\text{m}$, $\Delta\lambda=1.6\mu\text{m}$). T-ReCS utilizes a Raytheon 320×240 pixel Si:As IBC array which is optimized for use in the $7\text{--}26\mu\text{m}$ wavelength range. The pixel scale is $0.089''/\text{pixel}$, yielding a field of view of $28''.8\times 21''.6$. Co-added frames were saved every

10 sec, and the telescope was nodded every 30 sec. The co-added frames were examined individually during the data reduction process and those plagued by clouds (i.e., showing high and/or variable background or decreased source flux) were discarded. In both filters the northern and southern radio jet regions were imaged, yielding final mosaicked images with effective field of views of approximately $28''\times 35''$. The $8''$ overlapping region was used to register the northern and southern images of each mosaic. However, the individual images were cropped before they were mosaicked so the final mosaic has the same signal to noise across the whole image. The final *effective* exposure times for the mosaics presented here are therefore 140 sec at $11.7\mu\text{m}$ and 180 sec at $18.3\mu\text{m}$.

Flux calibration was achieved by observing the MIR standard star HD 169916 (λ Sgr) at similar airmasses to the G35.20-0.74 observations. The assumed flux densities for HD 169916 were taken to be 22.29 Jy at $11.7\mu\text{m}$ and 9.24 Jy at $18.3\mu\text{m}$. These assumed standard star flux densities were found by convolving the spectral irradiance templates of the stars from Cohen et al. (1999) with the given T-ReCS filter transmission profile. Derived flux densities for the entire region of G35.20-0.74 are measured to be 3.06 ± 0.09 Jy at $11.7\mu\text{m}$ and 46.87 ± 3.66 Jy at $18.3\mu\text{m}$ using a square aperture of $6''.9\times 13''.5$. These flux densities are quoted with their $1\text{-}\sigma$ total error, which is a quadrature addition of the statistical variation from the aperture photometry (due to the standard deviation of the background array noise) and the flux calibration error. The flux calibration error was found from the standard deviation of the variation of the standard star flux density in each co-added nod position. Since the science and standard star images were cleaned of any effects from clouds, the quoted errors are thought to be robust, however the errors were calculated using all available data. Comparisons to the lower angular resolution observations by De Buizer et al. (2005) show the values derived here to be consistent with

those derived in that previous work.

3. DISCUSSION

The mosaicked images at 11.7 and 18.3 μm are presented in Figure 1. These images are cropped to show only the parts of the field that have MIR sources. No significant MIR emission was detected outside these cropped areas at a 3- σ upper limit of 41 mJy-arcsec $^{-2}$ at 11.7 μm and 283 mJy-arcsec $^{-2}$ at 18.3 μm . Sources 1, 2, and 10 are seen at 11.7 μm but not at 18.3 μm , and source 3 is seen at 18.3 μm , but not 11.7 μm . Source 4 is marginally detected at 18.3 μm . The remaining sources are detected at both wavelengths and are mostly knots of emission associated with the MIR monopolar jet of G35.20-0.74. The origin of Figure 1 is the expected location of the outflow source itself. This source is a B2.6 star (as derived from the 8.5GHz flux density of Gibb et al. 2003 and using the method described in De Buizer et al. 2005) that can be seen as a UC HII region in the radio and has been dubbed G35.2N.

3.1. Relations to radio continuum and NIR emission

The MIR images were registered with respect to the NIR K and L' images of Fuller et al. (2001). Very accurate relative astrometry ($<0.15''$) was achieved because of the presence of three compact MIR sources (1, 2, and 4) that are also present in the K and/or L' images. The absolute astrometry of the NIR images (and, consequently, the MIR images) comes from matching up NIR point sources with their optical counterparts found in the USNO B1.0 astrometric catalog. The estimates of the 1- σ absolute uncertainty in these coordinates are 0.3'' for Right Ascension and 0.1'' for Declination.

Figure 2a shows the K emission (thick white contours) overlaid on the 11.7 μm image, and Figure 2b shows the L' emission (thin white contours) overlaid on the 18.3 μm image. The L' emission from the jet looks very similar to what is seen in the MIR. The K emission appears to be dominated more by the material in the north, further along the outflow axis, with very little emission down near the outflow source itself. The convex structure seen in the NIR breaks up into separate MIR components (knots 5 and 8), and therefore is probably not a bow-shock as implied by Fuller et al. (2001).

The L' images of Fuller et al. (2001) show what they claim is weak NIR emission from the southern jet of G35.20-0.74 (see Figure 2b). Interestingly, this emission is extremely weak at K, bright at L', not detected at 11.7 μm , but present at 18.3 μm (Source 3 in Figure 1).

The MIR images were also registered with respect to the high-resolution 8.5 GHz radio continuum images of Gibb et al. (2003) in Figure 2a (thin white contours), and with the low-resolution 15 GHz radio continuum image of Heaton & Little (1988) in Figure 2b (thick white contours). The 1- σ relative astrometric error between the MIR and radio continuum images is estimated to be 0.34'' in Right Ascension and 0.18'' in Declination. The MIR and NIR images and contours shown in Figure 2 have been shifted +0 $^{\circ}$ 023 (+0.35'') in Right Ascension to place G35.2N on the infrared outflow axis (this is approximately the estimated 1- σ astrometric uncertainty).

In Figure 2b it can be seen that the overall extent of the

northern radio lobe is comparable to the MIR emission. There is also considerable MIR emission coming from the central radio continuum emitting region near the outflow source, however there is no MIR emission from the southern radio peaks. G35.2N is also the location of one of the two millimeter peaks (Gibb et al. 2003) in this region (crosses in Figure 2b).

The two northernmost radio knots lie close to, but are not exactly coincident with MIR sources 6 and 7. For these knots, the radio and the MIR may be tracing slightly different emitting regions within the knots themselves.

3.2. Nature of the mid-infrared emission

MIR emission from outflows has been detected previously (e.g., Noriega-Crespo 2004), however these outflows have been claimed to be dominated by shock lines of H $_2$ contained within the filters used. For the observations presented here there are no H $_2$ lines within the bandpass of either the 11.3 or 18.3 μm filters. There is a possibility that there may be some contribution to the emission at 11.7 μm because of PAH emission, however this is not a concern at 18.3 μm . The steeply rising spectral slope from L' to 18.3 μm of the narrow, elongated infrared emission coincident with and immediately north of the position of G35.2N demonstrates that the infrared emission here is dominated by longer wavelength continuum emission. Therefore the nature of the infrared emission is concluded to be dominantly continuum dust emission from the outflow cavity walls. This cavity was created by the molecular outflow punching a hole in the dense molecular material surrounding young stellar source at the center of G35.20-0.74. The central source is mostly likely directly heating the walls of this cavity. The northern lobe of the outflow was found to be slightly blueshifted towards Earth (i.e., in CO by Gibb et al. 2003; in CI by Little, Kelly, & Murphy 1998). Given this fortuitous geometry, we can see directly into the outflow cavity itself due to the outflow clearing away the material along our line of sight.

The sources further north of G35.20-0.74, namely sources 5-9, are expected to be knots of dust either in the outflow itself of clumps of pre-existing material that are being impinged upon by the outflow. Source 6 lies 19200 AU from G35.2N and is still at an estimated dust color temperature of 112 K. This is based on the 11.7 and 18.3 μm flux densities of this source and neglecting the possible effects of silicate absorption (see De Buizer et al. 2005 for method and limitations). What is heating the dust this far out? Smaller dust grains can be heated out to farther distances than large dust grains. The typical size range of interstellar grains is believed to be 0.003-10 μm , and typical grain compositions include smooth astronomical silicates, graphite, and silicon carbide (Laor & Draine 1993, Draine & Lee 1984). For the following I will use the equation for dust temperature given by Sellgren, Werner, & Dinerstein (1983) and the ultraviolet and infrared emissivities of Draine & Lee (1984). Assuming the dust is made up of smooth astronomical silicates, dust with a lower limit size of 0.003 μm can be heated to 112K only out to \sim 16000 AU by a B2.6 star. If the dust is made of graphite, one can heat out to the distance of source 6 with grains having a typical size of 0.005 μm , still near the lower limit size. However, if silicon carbide is the assumed composition of the dust,

then one can get heating out much farther than source 6, namely ~ 52000 AU at the $0.003 \mu\text{m}$ lower limit size. There is a possibility of some contribution from shock heating, although Fuller et al. 2001 claim no detection of shock-excited H_2 in the region. Beaming of the MIR emission along the outflow axis, rather than the isotropic emission assumed in the above calculations, could also help in heating grains farther out. Interestingly, the MIR luminosity derived from the dust color temperature gives an estimated value of $1.6 \times 10^3 L_\odot$. Assuming the MIR luminosity is all the luminosity of the source (an obvious underestimate) and calculating a spectral type from that bolometric luminosity using the method of De Buizer et al. (2005) gives a value of $\sim \text{B3}$, consistent with the radio derived spectral type. In summary, all of the dust, even as far out as source 6, *can* indeed be heated directly by G35.2N, depending on dust composition and size (as well as beaming), though we cannot rule out contributions from other possible heating mechanisms.

As discussed in the previous section, MIR source 3, coincident with NIR emission from the presumed infrared southern counterjet, does not have a smoothly increasing spectral slope typical of dust continuum emission, but instead is only present at L' and $18.3 \mu\text{m}$. This implies that the emission in this southern source is dominated by line emission of some kind. The usual suspects are: 1) H_2 emission from shocks, however, Fuller et al. (2001) claim no detection of H_2 in the region; 2) PAH emission from the photo-dissociation region of the outflow interface with the molecular cloud, however the L' and $18.3 \mu\text{m}$ filters do not encompass any PAH features; 3) $[\text{FeII}]$ emission from shocks. This last one may be a possibility since $[\text{FeII}]$ lines are found in both filter bandpasses, but spectroscopy will be needed to know for sure.

3.3. Masers

The positions of the OH masers from Hutawarakorn & Cohen (1999) and water masers from Forster & Caswell (1989) are shown in Figure 2c (asterisks and X symbols, respectively). The positions of these maser sources with respect to the radio continuum emission were taken from Gibb et al. (2003). There are also methanol masers plotted in Figure 2c (large crosses), that were found by A.G. Gibb (private communication), and have positions known to $0.2''$ with respect to the radio continuum.

Interestingly, the combined distribution of the masers is in a V-shape, with its apex near the G35.2N source itself. From their positions with respect to the near and MIR emission, the masers appear to be tracing the outflow cavity walls. In the case of the OH and water masers, they may be excited to emit here by the slower oblique shocks created by the outflow on the cavity walls. Methanol masers on the other hand are believed to be excited by MIR radiation (i.e., Sobolev & Deguchi 1994; Sobolev, Cragg, & Godfrey 1997). The copious amount of MIR emission associated with this outflow source implies that at least the pumping mechanism needed for the generation of methanol masers exists on such outflow cavity walls.

Given the narrow opening angle of this outflow cavity

as seen in the MIR and the fact that methanol masers are often found in linear distributions (e.g. Norris et al 1993), it is possible that methanol masers in general are associated with the cavities walls of outflowing young massive stars. Previous observations by De Buizer (2003) found the majority of linear methanol maser distributions in that sample were found at position angles similar to H_2 emission expected to trace outflows from the host YSOs. Furthermore, other sources like NGC 7538 IRS 1 (De Buizer & Minier 2005) have been observed in the MIR to have outflow-like MIR emission at the same position angle as other outflow indicators (CO in the case of NGC 7538 IRS1), as well as having a linear methanol maser distribution at a similar position angle as well. All of this may point to a scenario where the linearly distributed methanol masers may be associated more generally with outflows of massive YSOs, and not with circumstellar disks as was previously thought (i.e. Norris et al 1993).

3.4. Implications for mid-infrared bright YSOs

There is a tendency to think that if MIR emission is detected in a young stellar object (especially if it appears elongated in its morphology) that it is emission from a circumstellar disk (i.e. Lada & Lada 2003). Recent observations and theories (e.g., Miroshnichenko et al. 1999) have shown that, at least for the more massive YSOs, the dominant source of MIR emission comes from an accretion envelope. These accretion envelopes may be elongated as well (De Buizer, Osorio, & Calvet 2005). The observations presented here show that we must take in to account another source of elongated MIR emission. On a 3-4m telescope (De Buizer et al. 2005), or with the resolution of the *Spitzer Space Telescope*, the MIR emission from this G35.20-0.74 could be misinterpreted as a circumstellar disk. Only recently with the increase of MIR instruments on 8-10m telescopes have we begun to resolve source like G35.20-0.74 with such detail as to discern their true MIR emission as being outflow-related (e.g., NGC7538 IRS 1; De Buizer & Minier 2005).

Therefore one must be cautious when trying to infer disk properties from unresolved or partially resolved sources since the outflow cavities of YSOs can be the dominant source of MIR emission. On the other hand, the mere presence of such outflow cavities with small opening angles implies the presence of collimating accretion disks at the bases of the outflows. So while MIR emission may not always be a *direct* tracer of circumstellar disks and their properties, the presence of such emission in the near circumstellar environment of YSOs may still indirectly indicate the presence of a disk.

Based on observations obtained at the Gemini Observatory, which is operated by AURA, Inc., under a cooperative agreement with the NSF on behalf of the Gemini partnership: the NSF (U.S.), the PPARC (U.K.), the NRCC (Canada), CONICYT (Chile), the ARC (Australia), CNPq (Brazil) and CONICET (Argentina). I would also like to thank James Radomski for his illuminating discussions which helped in the writing of this article.

REFERENCES

- Beuther, H., Schilke, P., Sridharan, T. K., Menten, K. M., Walmsley, C. M., & Wyrowski, F. 2002, *A&A*, 383, 892
- Cohen, M., Walker, R. G., Carter, B., Hammersley, P., Kidger, M., & Noguchi, K. 1999, *AJ*, 117, 1864
- De Buizer, J. M., Radomski, J. T., Telesco, C. M., & Piña, R. K. 2005, *ApJS*, 156, 179
- De Buizer, J. M., & Minier, V. 2005, *ApJ*, 628, L151
- De Buizer, J. M. 2003, *MNRAS*, 341, 277
- Forster, J. R., & Caswell, J. L. 1989, *A&A*, 213, 339
- Fuller, G. A., Zijlstra, A. A., & Williams, S. J. 2001, *ApJ*, 555, L125
- Gibb, A. G., Hoare, M. G., Little, L. T., & Wright, M. C. H. 2003, *MNRAS*, 339, 1011
- Heaton, B. D., & Little, L. T. 1988, *A&A*, 195, 193
- Hutawarakorn, B., & Cohen, R. J. 1999, *MNRAS*, 303, 845
- Lada, C. J., & Lada, E. A. 2003, *ARA&A*, 41, 57
- Little, L. T., Kelly, M. L., & Murphy, B. T. 1998, *MNRAS*, 294, 105
- Miroshnichenko, A., Ivezić, Ž., Vinković, D., & Elitzur, M. 1999, *ApJ*, 520, L115
- Noriega-Crespo, A., et al. 2004, *ApJS*, 154, 352
- Norris, R. P., Whiteoak, J. B., Caswell, J. L., Wieringa, M. H., & Gough, R. G. 1993, *ApJ*, 412, 222
- Sellgren, K., Werner, M. W., & Dinerstein, H. L. 1983, *ApJ*, 271, L13
- Shepherd, D. S., & Churchwell, E. 1996, *ApJ*, 457, 267
- Sobolev, A. M., & Deguchi, S. 1994, *A&A*, 291, 569
- Sobolev, A. M., Cragg, D. M., & Godfrey, P. D. 1997, *A&A*, 324, 211
- Zhang, Q., Hunter, T. R., Brand, J., Sridharan, T. K., Molinari, S., Kramer, M. A., & Cesaroni, R. 2001, *ApJ*, 552, 167

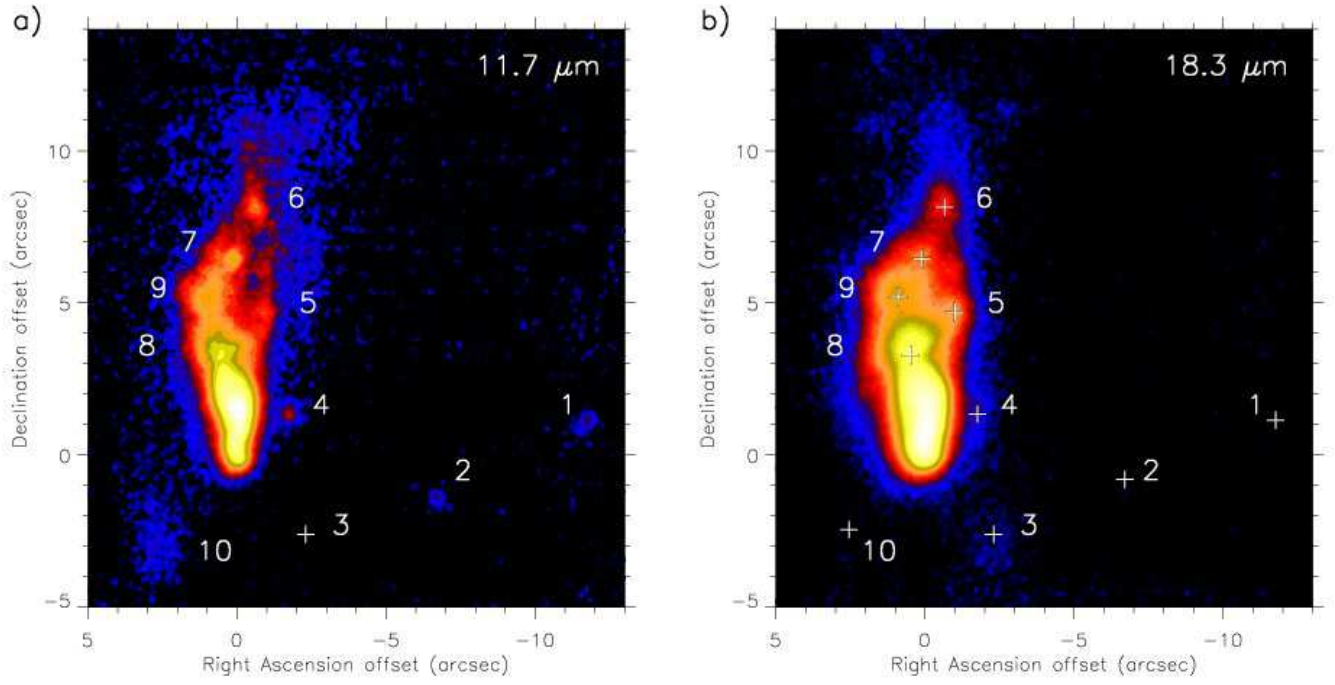


FIG. 1.— The region of G35.20-0.74 in false-color as seen at a) $11.7\ \mu\text{m}$ and b) $18.3\ \mu\text{m}$ with T-ReCS. Crosses in b) show the locations of individual MIR sources at $11.7\ \mu\text{m}$ and are numbered by increasing right ascension. The cross in a) shows the $18.3\ \mu\text{m}$ location of source 3 which is not seen at $11.7\ \mu\text{m}$.

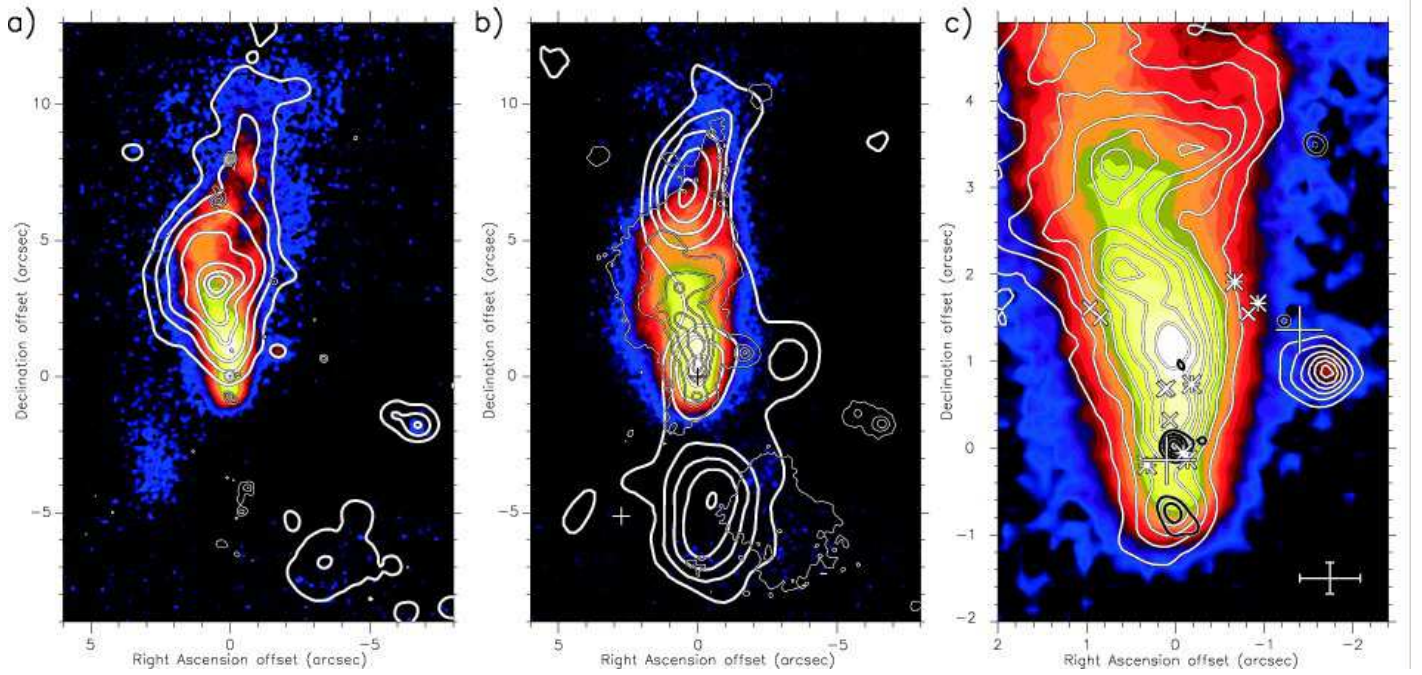


FIG. 2.— The G35.20-0.74 jet as seen at different wavelengths. Panel a) shows the 11.7 μm image in false-color overlaid by K-band emission of Fuller et al. (2001) as thick white contours, and the 8.5 GHz high resolution radio continuum emission of Gibb et al. (2003) as thin white contours. Panel b) shows the 18.3 μm image in false color overlaid by the low resolution 15 GHz radio continuum image of Heaton & Little (1988) as thick white contours, and L' image of Fuller et al. (2001) as the thin white contours. Panel c) is a zoom in on the central region of the 11.7 μm image in false-color, the L' contours in white and the high resolution radio continuum contours in black. OH maser of Hutawaraorn & Cohen (1999) are shown as asterisks, water masers of Forster & Caswell (1989) are shown as X symbols, and methanol masers of A. G. Gibb (priv. comm.) shown as large crosses. The cross in the lower right of panel c) shows the $\pm 1\text{-}\sigma$ relative astrometric uncertainty between the radio continuum and NIR.